From aggregative adsorption to surface depletion

Version Feb 20 2017

From aggregative adsorption to surface depletion: Aqueous systems of C_nE_m amphiphiles at hydrophilic surfaces

Gernot Rother,[1,2] Dirk Müter,[3] Henry Bock,[4*] Martin Schoen,[1] and Gerhard H. Findenegg[1*]

[1] *Stranski-Laboratorium für Physikalische und Theoretische Chemie, Institut für Chemie, Technische Universität Berlin, 10623 Berlin, Germany*
[2] *Geochemistry & Interfacial Science Group, Chemical Sciences Division, Oak Ridge National Laboratory, Oak Ridge, Tennessee 37831-6110, U.S.A.*
[3] *Nano-Science Center, Department of Chemistry, University of Copenhagen, Copenhagen, Denmark*
[4] *Institute of Chemical Sciences, Heriot-Watt University, Edinburgh, EH14 4AS, United Kingdom*

*corresponding authors: h.bock@hw.ac.uk, findenegg@mailbox.tu-berlin.de

Adsorption of a short-chain nonionic amphiphile (C_6E_3) at the surface of mesoporous silica glass (CPG) was studied by a combination of adsorption measurements and mesoscale simulations. Adsorption measurements covering a wide composition range of the C_6E_3 + water system show that no adsorption occurs up to the critical micelle concentration (cmc), at which a sharp increase of adsorption is observed that is attributed to ad-micelle formation at the pore walls. Intriguingly, as the concentration is increased further, the surface excess of the amphiphile begins to decrease and eventually becomes negative, which corresponds to preferential adsorption of water rather than amphiphile at high amphiphile concentrations. The existence of such a surface-azeotropic point has not previously been reported in the surfactant adsorption field. Dissipative particle dynamics (DPD) simulations were performed to reveal the structural origin of this transition from aggregative adsorption to surface depletion. The simulations indicate that this transition can be attributed to the repulsive interaction between head groups, causing depletion of the amphiphile in the region around the corona of the surface micelles.

Keywords: adsorption, mesoscale simulations, nanopores, surface azeotrope, surfactant

Introduction

Adsorption of surfactants onto solid surfaces from aqueous solutions has been studied extensively for decades, motivated by its relevance for technological processes involving wetting, adhesion, detergency, and related phenomena. It is well-established that the adsorption onto hydrophilic surfaces depends mostly on the strength of interaction of the surfactant head groups with the surface [1], and on the length of the hydrophobic surfactant tail [2]. If the free energy of binding of the head groups is too small to compensate for the entropy loss upon adsorption, no adsorption of single surfactant molecules occurs. At a concentration close to the critical micelle concentration (cmc) surfactant aggregates start to form at the surface and the adsorbed amount rises steeply until levelling off above the cmc. This aggregative adsorption behaviour is exemplified by nonionic surfactants at hydrophilic silica [2,3,4,5,6,7,8,9]. Surfactants of the n-alkyl poly(oxyethylene) monoether family, $C_nH_{2n+1}(OC_2H_4)_mOH$ (abbreviated as C_nE_m), are convenient model amphiphiles for such studies, because their amphiphilic character can be tuned by varying the lengths of the hydrophobic and hydrophilic blocks. For C_nE_m surfactants, hydrogen bonding of the ether groups to the surface silanol groups is believed to represent the dominant binding mechanism. However, since the ether groups of the surfactant as well as the surface silanol groups are strongly hydrated in water at ambient temperature, the net free energy of binding of the surfactant head groups to the surface is small.

Micelle formation of surfactants in aqueous media represents a hydrophobic aggregation with an entropic driving force, caused by the release of water from the hydrophobic hydration shell of the tails [10]. Accordingly, as the length of the hydrophobic tail is increased, the cmc is shifted strongly to lower concentrations: Whereas C_4E_1 is a *weak amphiphile* that forms micellar aggregates in water only at high concentrations (above 1 mol/L) [11], C_6E_3 and C_8E_4 represent *stronger amphiphiles* with well-defined cmc near 0.1 mol/L [12,13] and below 0.01 mol/L [7], respectively. Adsorption isotherms of C_8E_4 at silica surfaces exhibit the pronounced S-shape that is indicative of aggregative adsorption, with a critical surface aggregation concentration (csac) of (0.7-0.9) x cmc [7,9]. Conversely, water is

preferentially adsorbed from aqueous solutions of C_4E_1, corresponding to a *negative* surface excess of this weak amphiphile at silica surfaces [14].

To better understand the influence of amphiphilic strength on amphiphile adsorption at hydrophilic surfaces, and to bridge the gap between the vastly different concentration regimes of micellar aggregation of C_8E_4 and C_4E_1, we have now studied the adsorption behaviour of the C_6E_3 + water system over a wide composition range. We find that C_6E_3 indeed shows aggregative adsorption near its cmc. However, at higher concentrations the adsorbed amount, expressed as the surface excess of the amphiphile, decreases and eventually becomes negative beyond a pore-size dependent surface-azeotropic concentration. To our knowledge such a behaviour has not been reported previously for surfactant solutions.

In adsorption from binary liquid mixtures a surface azeotropic point represents a composition of the bulk mixture at which the reduced surface excess amount is passing from positive to negative values. The occurrence of a surface azeotrope is well-understood for strongly heterogeneous surfaces, when one component is preferred by one type of surface sites and the other component by the other surface sites [15]. For energetically more uniform surfaces, as in the present case, it has long been recognized that surface azeotropy may occur for mixtures exhibiting strong positive deviations from ideality, particularly at temperatures close to liquid/liquid phase separation [16,17,18]. C_nE_m + water systems indeed undergo phase separation into water-rich and amphiphile-rich phases at temperatures above a lower critical solution temperature T^c. The phase diagram of the C_6E_3 + water system is shown in Figure 1. However, the origin of surface azeotropy in this system seems to be different from the situation considered in the literature, as the nature of the molecular interactions is more complex and the surface azeotrope is observed not only at temperatures close to T^c.

To uncover the cause of the surface azeotrope we complement our experimental study with molecular simulations using Dissipative Particle Dynamics (DPD) of a bead-spring model of amphiphilic chain molecules consisting of hydrophilic head beads and hydrophobic tail beads in an implicit solvent. This model has been shown to correctly reproduce the behaviour of aqueous solutions of non-ionic

amphiphilic chain molecules in the bulk [19], near interfaces [20], and in confinement [21,22,23,24]. The model amphiphile is studied in a cylindrical pore that is physically connected to a bulk reservoir. This set-up has two consequences. First, an interface between bulk and confined fluid exists and, second, at thermodynamic equilibrium the chemical potential in bulk and in confinement is equal. For hydrophilic pores that have a moderate preference for the head-groups, the simulations reproduce the existence of a surface azeotrope at higher amphiphile concentrations, and provide insight into the subtle interplay between aggregation and adsorption of the amphiphile in the pore space that causes the appearance of the azeotrope.

Experimental system and results

Adsorption from the C_6E_3 + H_2O system was studied for three controlled-pore glass ("CPG-10") materials with nominal pore sizes 75 Å, 240 Å, and 500 Å, denoted here as CPG-75, CPG-240 and CPG-500, respectively. A characterization of these materials and details of their pre-treatment are presented elsewhere [9,14]. For comparison with the simulation data the measured mean pore diameters d_p of the three materials (10.3, 35, and 50 nm [14]) can be expressed in terms of the apparent diameter of C_6E_3 micelles, d_m = 3.7 nm [25], giving d_p/d_m = 2.8, 9.5, and 13.5, respectively. C_6E_3 from Bachem (>98% GC) and milli-Q50 water was used to prepare the aqueous mixtures.

To determine the adsorption behaviour over a wide composition range, adsorption isotherms were measured by an isothermal titration technique, i.e. stepwise addition of small aliquots of a surfactant solution and determination of the equilibrium concentration of the supernatant solution by means of a sensitive differential refractometer. Separate measurements with dilute titrant solutions were performed for the low-concentration regime to reach highest sensitivity. The adsorbed amount is expressed as the (mass-related) reduced surface excess concentration of the amphiphile (A)

$$\Gamma_A^{(m)} = \frac{m^0(w_A^0 - w_A)}{M_A m_s a_s} \qquad (1)$$

where m^0 is the mass of liquid mixture with an initial amphiphile mass fraction w_A^0 and final mass fraction w_A, after equilibration with a mass m_s of the porous glass of specific surface area a_s. The reduced surface excess concentration of water (W) is related to $\Gamma_A^{(m)}$ as $\Gamma_W^{(m)} = -(M_A/M_W)\Gamma_A^{(m)}$, where M_A and M_W represent the molar mass of the amphiphile and water, respectively, and M_A/M_W = 13.0 for C_6E_3. In the present system the two components have similar densities (ρ_{C6E3} = 0.964 g/cm^3, ρ_W = 0.998 g/cm^3 at 20°C). In this case, the mass fraction w_A becomes similar in magnitude to the volume fraction of amphiphile, ϕ_A, and the reduced surface excess concentration $\Gamma_A^{(m)}$ obtained in the experiments becomes similar in magnitude to the (volume-related) reduced surface excess concentration [26], $\Gamma_A^{(v)}$, which is accessible in the molecular simulations. For this reason, the superscripts (m) or (v) in the symbol of the surface excess concentration are omitted in the rest of this paper.

Figure 2 shows isotherms of the surface excess Γ_A of C_6E_3 in CPG-240 for several temperatures below and above the lower critical solution temperature (T^c = 44.1°C). All isotherms exhibit the characteristics of aggregative adsorption [3,27], viz., no adsorption at low concentration and a sharp onset of adsorption at a csac. The csac decreases with increasing temperature. The isotherms for temperatures up to T^c reach a maximum at concentrations not far above the csac, and the level of maximum adsorption increases with temperature as the phase separation temperature is approached. The two isotherms for temperatures $T > T^c$ exhibit no maximum but the adsorption increases without limit above the csac. At these temperatures, phase separation of the bulk mixtures occurs at concentrations shortly above the cmc (see phase diagram in Fig. 1). By analogy with the pore condensation of pure fluids near liquid-vapour coexistence [28], we attribute the sharp increase in Γ_A in the isotherms for temperatures $T > T^c$ to a shifted phase transition in the pores. A detailed discussion of this behaviour is postponed to a subsequent publication.

The adsorption isotherms of C_6E_3 in the low-concentration regime shown in Figure 2 resemble those found for C_8E_4 in the same CPG material [9], but since C_6E_3 is a weaker amphiphile than C_8E_4, micelle formation and surface aggregation occur at much higher concentrations than for C_8E_4. Values

of the csac extracted from the adsorption isotherms in Fig. 2 are on average 20% smaller than the cmc values at the same temperature given in the literature [12,13]. This is consistent with the behaviour found for the stronger amphiphile C_8E_4 [7,9].

Adsorption isotherms of the C_6E_3 + H_2O system in the three CPG materials are shown for a wider range of compositions w_A in Figure 3. It can be seen that the surface excess Γ_A after passing the maximum decreases steadily with increasing w_A and eventually changes from positive to negative values at a surface-azeotropic composition w_A^{az}. Surface-azeotropy is rather unusual and its appearance for surfactant + water systems may, at first sight, be unexpected. However, considering that the surfactant chemical potential changes only slowly with concentration beyond the cmc, it must be expected that adsorption essentially stops and therefore, the surface excess begins to decrease, which may eventually lead to its sign inversion. The 'rate' of decrease, $-d\Gamma_A/dw_A$, depends strongly on the pore size (Figure 3). Intriguingly, the rate of decrease is largest for the CPG material with the widest pores (CPG-500) and smallest for the material with smallest pores (CPG-75). This is reflected in the pronounced decrease of the azeotropic composition with increasing pore size: w_A^{az} = 0.27 (CPG-75), 0.20 (CPG-240) and 0.11 (CPG-500). In the material with widest pores (50 nm) the surface azeotrope is located at a bulk composition lower than the critical composition of liquid/liquid phase separation (w_A^c = 0.14; cf. Fig. 1). The pronounced influence of the pore size on the sign and magnitude of Γ_A at amphiphile-rich bulk compositions (see Fig. 3) suggests that the size and/or packing of the surface aggregates is affected by surface curvature and confinement. It is plausible that micellar packing effects may limit the adsorbed amount at least in CPG-75, where the mean pore diameter corresponds to less than 3 micellar diameters of C_6E_3. However, such confinement effects alone can not explain the pronounced dependence of the azeotropic composition on pore size.

A decrease in surfactant adsorption with increasing bulk concentration beyond the cmc has been reported in some studies for cationic surfactants adsorbed onto flat surfaces [29,30,31,32]. However, in all these cases the effect could be observed only when impurities were present, and it was limited to concentrations not far above the cmc. The effects reported here are different from

those in the literature in several respects: (1) C_6E_3 exhibits S-shaped isotherms with a well-defined and temperature-dependent plateau near the cmc, consistent with literature reports for other C_nE_m surfactants at silica surfaces [2-9]; (2) the decrease in surface excess extends over a wide concentration range and leads to a surface azeotrope; (3) the composition of the surface azeotrope exhibits a pronounced dependence on the pore size. Indeed, below we show that the occurrence of a surface azeotropic point can be reproduced by molecular simulation of an impurity-free system.

Mesoscale simulations

Computer simulations were performed to elucidate the nature of the surface azeotrope and its unusual pore size dependence. Mesoscale simulations of surfactant self-assembly in cylindrical pores were performed up to high bulk concentrations of the surfactant, using DPD simulations in the canonical ensemble (N,V,T) as reported previously [22]. The amphiphilic molecules were modelled as a chain of 5 hydrophilic head beads and 5 hydrophobic tail beads of equal diameter σ joined by springs. Tubular pores were represented by a hollow cylinder with smooth walls, directly connected to a bulk reservoir at both ends. The nominal pore radius R = 20 σ is equivalent to approximately four micelle diameters, making this system comparable to CPG-75. The pores are 130 σ long, with a transition region of 5 σ being ignored at either end, leaving a total length of 120 σ. As it is notoriously difficult to determine the location of interfaces in nanoscale systems, the location of the boundary of the pore volume in the radial direction is somewhat ambiguous. This has no impact on any of the *effects* studied here, but it does influence the exact location of the surface azeotrope. Here we assume that the cylindrical pore volume has a radius of about 19.5 σ, i.e. the pore volume ends approximately 1/2 σ before the location of the centres of the (averaged out) wall beads at R = 20 σ.

Due to the implicit treatment of the solvent and the use of a coarse-grained surfactant model, the beads interact via effective potentials [21]. The hydrophobic interaction between tail beads is attractive, all other bead-bead interactions are purely repulsive. The attractive interaction between

tail beads is represented by the Lennard-Jones (LJ) (12,6) potential, the repulsive interaction between head-head and head-tail segments by the WCA potential (i.e., the LJ potential shifted by +ε and truncated at the distance $r_{min} = 2^{1/6}\sigma$). As reported earlier [21], this model surfactant aggregates to spherical micelles at a cmc = 5.2x10^{-5} molecules/σ^3.

The smooth pore wall interacts with the hydrophilic head beads via a LJ potential, and with the hydrophobic tail beads via the corresponding WCA potential. The strength parameter for the attractive interaction of the head beads with the pore wall, ε_w (expressed relative to ε, the depth of tail-tail potential), represents the key parameter in this model, as it quantifies the preference of the pore wall for the head beads compared to the (implicit) solvent (water). An earlier study carried out using ε_w = 2.5 (i.e., a value representing a strong preference of the pore wall for the head groups) found an adsorption isotherm exhibiting the pronounced S-shape that is indicative of aggregative adsorption at a csac, which was located below the cmc [22]. For the present study the value for ε_w was reduced to 1.5, to simulate a system in which the pore wall does not show strong preference for the head beads of the amphiphile and therefore does not dominate the adsorption behaviour. The total number of amphiphile molecules N_p in the pore as a function of bulk amphiphile concentration C_b is shown in Figure 4a. Initially, N_p increases quickly with C_b as expected for the preferentially adsorbed species. At concentrations C_b > 2x10$^{-3}\sigma^{-3}$ the increase is slower and nearly perfectly linear. If this is compared to the hypothetical reference case where the entire pore volume is filled with bulk solution, $N_{ref}(C_b) = V_p C_b$ (red line in Figure 4a), one immediately realizes that N_p increases slower than N_{ref}, which eventually must lead to a crossover of the two lines. This crossing point is equivalent to the azeotropic point observed in the experiments. This is more easily seen when the simulation data are plotted as an excess compared to the reference just introduced. Here we define a (number-of-molecules based) surface excess via

$$\Gamma_A = \left(N_p - N_{ref}\right)/A_p \quad . \tag{2}$$

where the surface area of the cylindrical pore volume is $A_p = 2\pi RL$ with R =19.5 σ.

In figure Figure 4b, Γ_A is shown as a function of the bulk concentration. This surface excess isotherm is to be compared with the experimental isotherms in Fig. 3. Turning at first to the low-concentration region of the model isotherm, we note that $\Gamma_A(C_b)$ starts from the origin as a simple monotonic function up to concentrations far beyond the cmc ($5\text{x}10^{-5}\sigma^{-3}$). The absence of a csac implies that micelles rather than individual molecules adsorb in the model system. This result deviates from the experimental findings for C_6E_3, where csac ≈ cmc (Fig. 2). However, because surface aggregation below the cmc was observed in the simulations for the same surfactant model with ε_w = 2.5 [22], the absence of aggregative adsorption below the cmc can be attributed to the low adsorption parameter chosen in the present work (ε_w = 1.5).

For higher concentrations C_b the simulations confirm the experimental finding that the surface excess passes a maximum and decreases in a nearly linear manner at higher concentrations. The surface excess changes from positive to negative values at the azeotrope $C_b^{az} \approx 0.028\sigma^{-3}$. Because the effective volume of a molecule consisting of 10 beads is approximately $10(1/2)\sigma^3$, this corresponds to a volume fraction of amphiphile $\phi_b^{az} \approx 0.14$, which is in line with the values obtained in the experiment ($\phi_A^{az} \approx w_A^{az}$ from 0.11 to 0.27, depending on pore size; cf. Fig. 3).

Whereas the total number of amphiphile molecules in the pore (and the respective surface excess number) is directly accessible in the molecular simulations, the number of *adsorbed molecules* is not. Any proximity (e.g. to the pore wall) criterion to identify adsorbed molecules and aggregates breaks down at high concentrations, where amphiphile molecules may be found near the pore wall even if the pore fluid was entirely bulk-like. Moreover, the linear increase of N_p with C_b for $C_b > 2\text{x}10^{-3}\sigma^{-3}$ suggests that some part of the pore fluid behaves bulk-like.

Inspired by this observation we make the ansatz that some of the molecules in the pore are adsorbed (N_p^a), while the remaining are bulk-like (N_p^b), i.e. $N_p = N_p^a + N_p^b$. If we assign specific regions of the pore volume to the two types of behaviour, we obtain the *adsorbed-layer model*. The contribution of the bulk-like molecules can be expressed as $N_p^b = C_b V_p^b$. For the adsorbed molecules we assume that they conform to the Langmuir model, consistent with our earlier conclusion that for

the chosen low adsorption parameter (ε_w = 1.5) we don't find aggregative adsorption but rather the adsorption of aggregates. The concentration dependence of the number of molecules in the pore can then be written as

$$N_p(C_b) = N^* \frac{kC_b}{1+kC_b} + V_p^b C_b \qquad (3)$$

where N^* and k are parameters of the Langmuir equation.

A good fit of the simulation data $N_p(C_b)$ is obtained with N^*= 579, k = 2533 σ^3, and V_p^b = 1.23x10^5 σ^3, as shown by the full curves in Figs. 4a and 4b. Because the total pore volume, $V_p = \pi R^2 L$, is 1.42x10^5 σ^3, the adsorbed-layer model implies that the adsorption volume V_p^a that is enriched or depleted of amphiphile represents about 15% of the pore volume, while in 85% of the pore volume the concentration of amphiphile changes as if it was bulk fluid. It is intriguing that only such a small part of the pore volume should be non-bulk-like for this relatively small pore (diameter approx. 4 micelle diameters).

A much clearer picture of the structural origin of the azeotrope is provided by radial density profiles. A set of radial densities for four different bulk concentrations is provided in Figure 5a. It is instructive to compare the radial density at the highest concentration to the snapshot in Figure 6. Clearly visible is a distinct ring of micelles near the pore wall and a channel of micelles in the centre of the pore, separated by a region of low amphiphile density. At low concentrations, a large proportion of the micelles is located near the pore wall, while the pore centre is depleted compared to the bulk density (dashed lines in Figure 5a). As the bulk concentration increases, more micelles accumulate near the wall, leading to an increase of the local density in this region. Eventually also the centre of the pore gets filled with micelles, but a depletion region remains between the micelles in the centre and those near the pore wall.

This depletion region is void of surfactant tail groups and only occupied by head groups (Figures 5b and 6). The relatively low head-group density in this micellar corona region (compared to

the high density of tail groups in the micellar core) is expected and originates from the repulsive interactions between head groups. This repulsion is also the most plausible reason why at low concentrations the pore centre is depleted. Inspection of Figures 5b and 6 reveals that there is a second depletion region near the pore wall, which is only interrupted by a peak of very high head-bead density stemming from adsorbed head beads. Because the radial densities represent only the location of bead centres, the pore volume and therefore the depletion region continues beyond the peak of adsorbed head beads towards the pore wall. The exact boundary is somewhat ambiguous, but defining it at R = 19.5 σ is reasonable (see discussion above).

The sequential appearance of the two maxima in the local density is also clearly visible in the contour plots in Figure 7. In particular, Figure 7b shows the difference between the actual local density and the corresponding bulk density. It can be seen that initially micelles near the pore wall cause a positive excess density while the rest of the pore is depleted. Interestingly, the excess density near the pore wall increases only weakly as the bulk density increases, which is consistent with our earlier observation that only a comparatively small number of molecules is actually adsorbed. At intermediate concentrations the concentration of micelles in the central region of the pore increases quickly and causes a high positive excess density. We attribute this to 1D ordering of micelles along the pore axis. However, this high local density is associated to only a small volume and therefore accounts only for relatively few molecules. This can be seen in Figure 5c, where the number of molecules located at a given distance from the pore centre is presented. It is immediately obvious that the micelles near the pore centre make only a small contribution to the total number of molecules in the pore and account only for a small positive deviation from the reference where the pores is filled with bulk solution (Figure 5d). For the highest bulk density chosen in this study this positive deviation is over-compensated by the inner depletion layer, then becomes positive again due to the micelles near the pore wall, and is over-compensated yet again by the outer depletion layer. Thus, the depletion layers caused by head/head repulsion and ordering of the micelles in a layer near the pore wall are the cause for the observed surface azeotrope.

The distinct and unexpected pore-size dependence of the azeotrope observed in the experiments (Figure 3) is now also plausible. Whereas the formation of a layer of micelles near the pore wall will always occur for sufficiently large pores, the associated change in curvature controls the fractions of pore volume associated to the individual depletion and accumulation regions. In addition, as the pore radius increases, the ordering of micelles near the pore centre will disappear, making this region more bulk-like. As a consequence, the volume of the inner depletion region should increase disproportionally with increasing pore size, causing a lowering of the surface-azeotropic composition.

Conclusions and Outlook

This study shows, in agreement with theoretical predictions [16,17,18], that for mixtures in which neither of the molecular species is strongly preferred by the surface, the adsorption behaviour can be dominated by the nature of interactions among the two species. Specifically, in aqueous solutions of nonionic surfactants, hydrophobic aggregation of the surfactant tails can be promoted by the presence of a hydrophilic surface, thus causing aggregative adsorption even if the surfactant molecules are not adsorbed in monomeric form. Whereas aggregative adsorption of surfactants at hydrophilic surfaces at concentrations near their cmc is a well-known phenomenon [1-9], the present study reveals an intriguing adsorption behaviour of such systems at concentrations well above the cmc. We find that a layer of micellar aggregates formed near the surface can repel further amphiphile molecules from the surface region, thereby causing a decrease in adsorption and formation of a layer depleted in amphiphile at higher amphiphile concentrations. On further increasing the bulk concentration this leads to a negative surface excess of the amphiphile above a surface azeotropic point. Our mesoscale simulations indicate that the formation of regions depleted in amphiphile is due to the repulsion between head groups of amphiphile molecules. For the family of C_nE_m amphiphiles this repulsion can be attributed to the strong hydration of the poly(oxyethylene) head groups. The resulting formation of a layer depleted in amphiphile at higher amphiphile concentrations is

reminiscent of the protein-resistant character of oligo(ethylene glycol) self-assembled monolayers [33].

As the effect originates from head/head repulsion which is common for all amphiphiles, it must be assumed that surface azeotropes may be found for many surfactant substrate systems. However, several important questions related to the observed adsorption behaviour remain open and need further studies. In particular, this concerns the following points:

(i) The relation between the csac and the adsorption parameter ε_w: Whereas a sharp surface aggregation concentration below the critical micelle concentration (csac < cmc) was found for our model amphiphile H5T5 in a previous study [22] for ε_w = 2.5, the present simulations with a weaker adsorption parameter, ε_w = 1.5, show that under these circumstances no adsorption occurs below the cmc, and adsorption of micelles starts at concentrations well above the cmc. Work with a shorter-chain model amphiphile and a range of ε_w values may help to clarify this point.

(ii) The influence of pore size on the azeotropic composition: In the earlier simulation study [22], performed for the same pore size as in the present work (R = 20 σ), a decrease in aggregate size with increasing hydrophilicity of the pore wall and an adsorption-induced increase of the effective head group area of the amphiphile at the pore wall was observed. It is of interest to find out to what extent these effects depend on the curvature of the pore walls and thus on the pores size. If the tendency of the surface micelles to flatten out is more pronounced at less curved surfaces, this may imply that amphiphile is repelled from a larger volume than in pores with higher surface curvature. This might explain the dependence of the azeotropic composition on the pore size observed in this work (Fig. 3).

(iii) The role of pore size relative to micelle size: For the chosen pore size we find that, in addition to a layer of surface micelles at the pore wall, a row of micelles appears in the core of the pore space at high amphiphile concentrations. Simulations with pores of smaller and larger size (in which either only one layer of micelles can form, or more than one row of micelles can be accommodated in the core

region of the pores) are needed to decide to what an extent the present simulation results are affected by the specific geometric conditions of this study.

(iv) The influence of temperature on the surface azeotrope and the depletion of amphiphile: Whereas the temperature dependence of adsorption in the low-concentration regime up to the cmc, and its relation to the liquid-liquid phase separation in C_nE_m + water systems, is now well-understood [9,27], the effect of temperature on the adsorption behaviour at high concentrations of amphiphile has not been considered in the literature. A program to study this and the other open questions by a combination of adsorption experiments and molecular simulation studies is in progress.

Acknowledgements

This work was supported by the German Research Foundation (DFG) in the framework of IRTG 1524 "Self-Assembled Soft-Matter Nanostructures at Interfaces". Analysis of experimental data and contribution to manuscript preparation by GR was supported by the Division of Chemical Sciences, Geosciences, and Biosciences, Office of Basic Energy Sciences, U.S. Department of Energy.

Figures

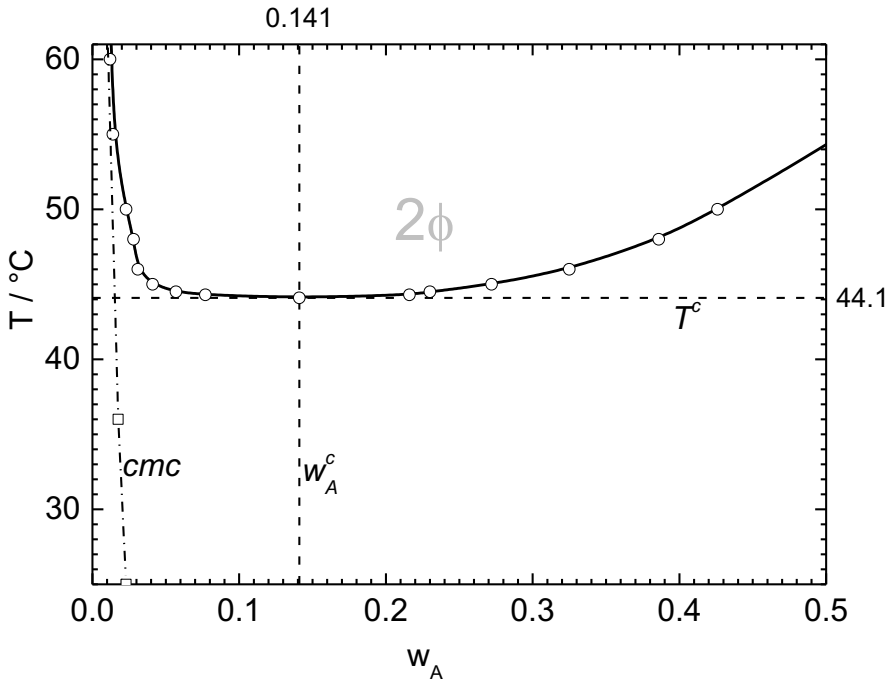

Fig. 1. Phase diagram of the C_6E_3 + H_2O system showing the locus of the cmc and the miscibility gap with its lower critical solution point. Sample composition is expressed by the mass fraction of amphiphile w_A.

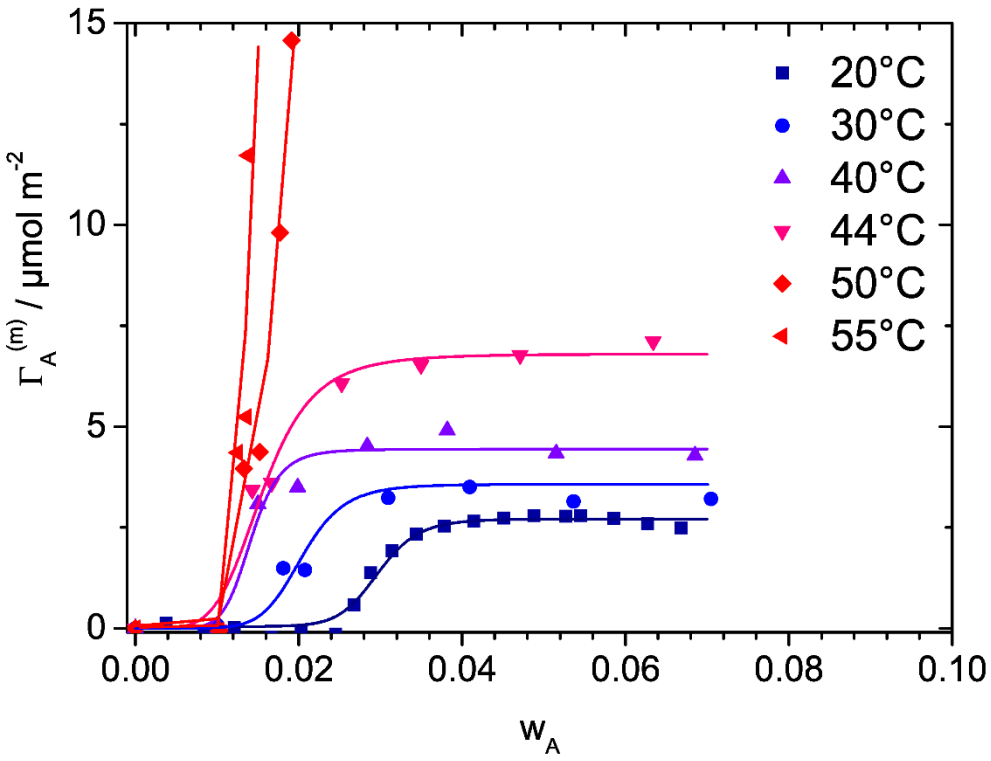

Fig. 2. Adsorption isotherms of C_6E_3 from dilute aqueous solutions on CPG-240, for temperatures below and above the critical temperature T^c = 44.1°C.

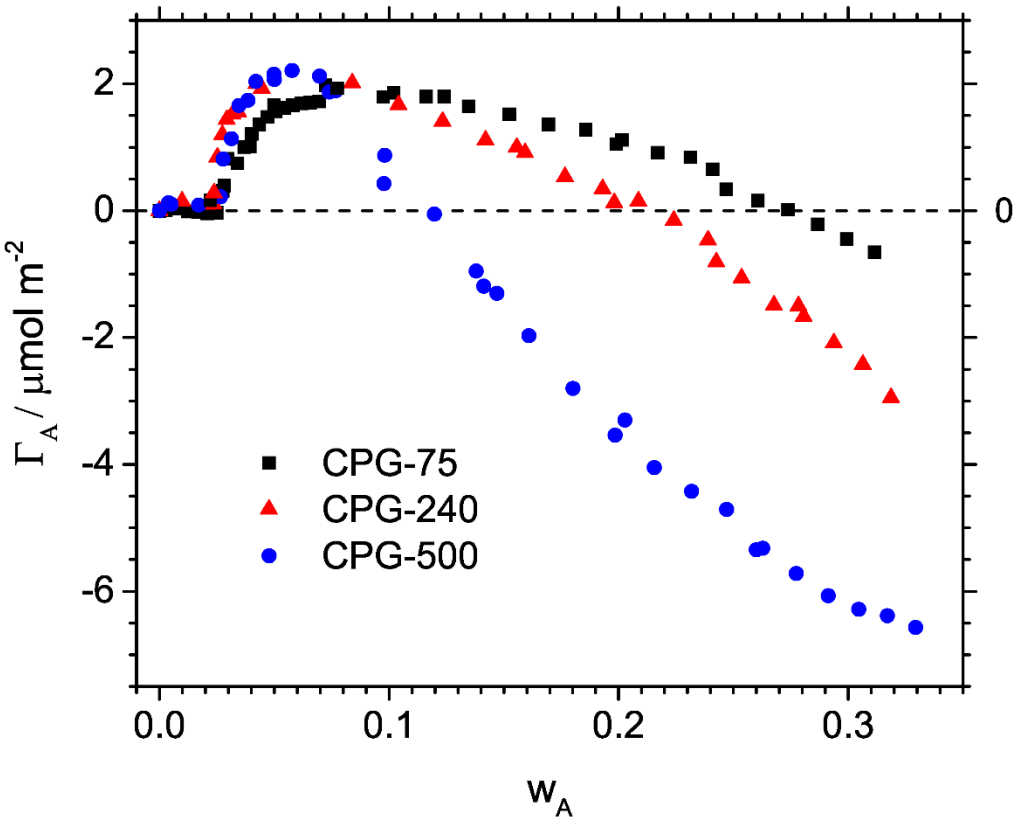

Fig. 3. Adsorption isotherms of C_6E_3 in the three CPG materials at 20°C, covering a wide range of amphiphile concentrations. The azeotropic point represents the composition at which the surface excess Γ_A changes from positive to negative values.

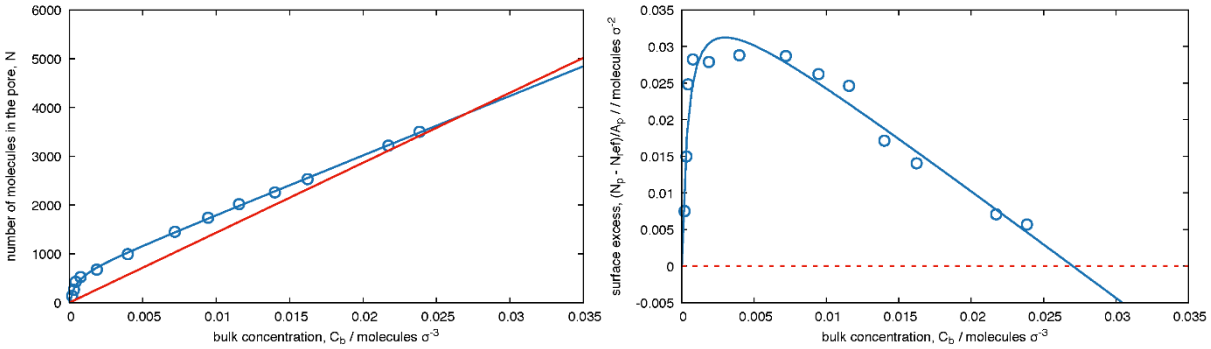

Figure 4: Isotherms from simulation. (a) The total number of molecules N_p as a function of bulk concentration C_b (circles) and a fit of the data for N_p to eq. (3) (blue line). Also shown is the reference system N_{ref}, where the pore is assumed to be filled by bulk solution (red line). (b) Surface excess concentration Γ_A given as the difference $N_p(C_b) - N_{ref}(C_b)$ normalized by the surface area of the pore (see eq. (2)).

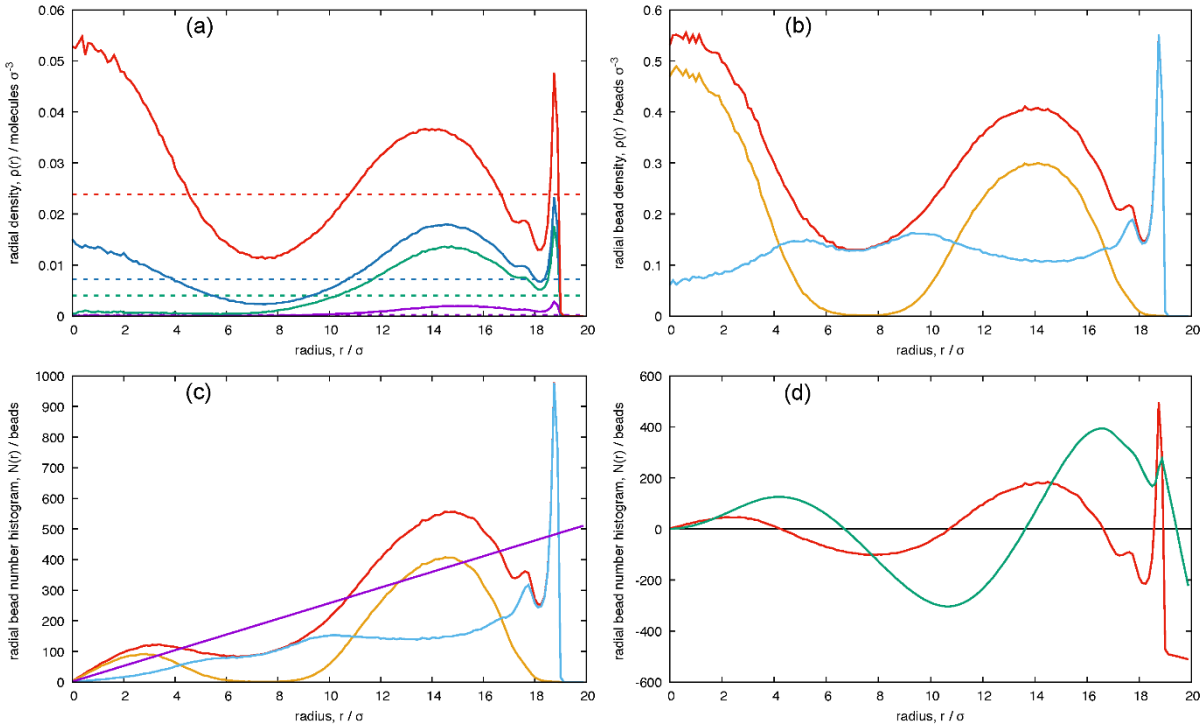

Figure 5: (a) Radial density profiles given as the local density of amphiphilic molecules as a function of radial position in the pore (0 denotes the pore centre) for four bulk concentrations $C_b = 0.00019\sigma^{-3}$ (red), $0.00398\sigma^{-3}$ (blue), $0.00718\sigma^{-3}$ (green), $0.0238\sigma^{-3}$ (magenta) also indicated in the figure (dashed lines). **(b)** Same as (a) for $C_b = 0.0272\sigma^{-3}$ but for the bead density and including the contributions from head (blue) and tail beads (yellow), to show that the two depletion regions around the surface micelles coincide with their head-group coronas. **(c)** Same as (b) but shown is the radial number of beads histogram, to indicate how many beads are present at a certain radius. The straight line (purple) indicates the reference case when the pore is filled with bulk solution. **(d)** Results of (c) expressed by the excess number of beads at a certain radius. Also shown is the accumulation of this property (green) to highlight how the depletion regions contribute to the total number of molecules in the pore. Note that the green curve passes through zero close to R < 19.5σ, indicating that the system has a bulk concentration near the surface azeotrope.

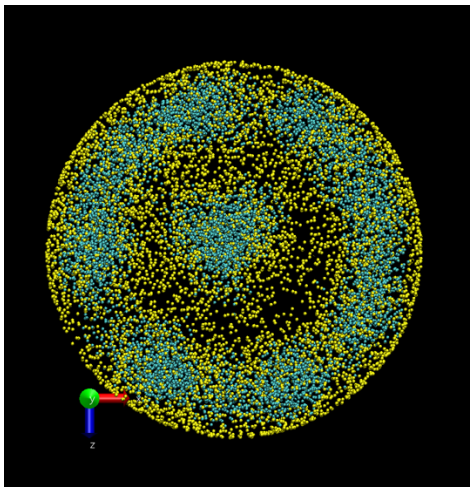

Figure 6: Snapshot of the simulation system at C_b= 0.157σ^{-3}. Shown is a thin slice perpendicular to the pore axis, blue and yellow spheres represent hydrophobic surfactant tail beads and hydrophilic surfactant head beads, respectively.

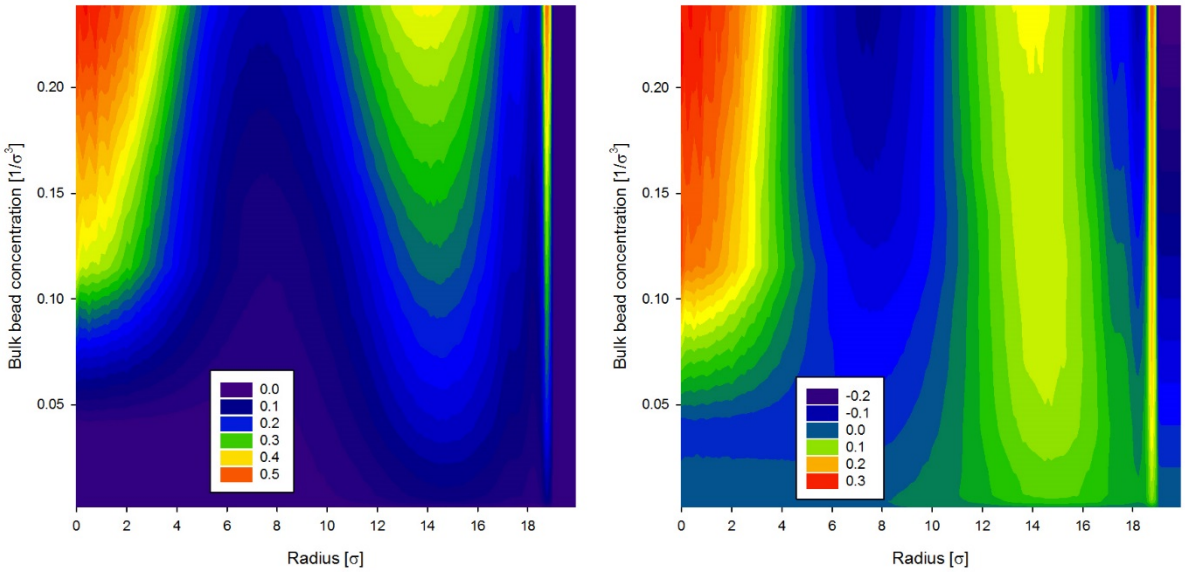

A b

Figure 7: (a) Radial densities of all beads as a function of concentration and **(b)** difference of the radial densities to the reference state to show how the depletion and accumulation regions evolve as the bulk concentration is increased.

References

[1] E. Tyrode, M.W. Rutland, and C.D. Bain, J. Am. Chem. Soc. **130**, 17434 (2008).
[2] F. Tiberg, J. Chem. Soc., Faraday Trans., **92**, 531 (1996).
[3] P. Levitz, and H. Van Damme, J. Phys. Chem. **90**, 1302 (1986).
[4] M. Lindheimer, E. Keh, S. Zaini, and S. Partyka, J. Colloid Interface Sci. **138**, 83 (1990).
[5] M.R. Böhmer, L.K. Koopal, R. Janssen, E.M. Lee, R.K. Thomas, and A.R. Rennie, Langmuir **8**, 2228 (1992).
[6] F. Giordano, R. Denoyel, and J. Rouquerol, Colloids Surf. A **71**, 293 (1993).
[7] Z. Kiraly, R.H.K. Börner, and G.H. Findenegg, Langmuir **13**, 3308 (1997).
[8] Y. Qiao, M. Schönhoff, and G.H. Findenegg, Langmuir **19**, 6160 (2003).
[9] O. Dietsch, A. Eltekov, H. Bock, K.E. Gubbins, and G.H. Findenegg, J. Phys. Chem. C **111**, 16045 (2007).
[10] V. Degiorgio, in *Physics of Amphiphiles, Micelles, Vesicles and Microemulsions*, edited by V. Degiorgio and M. Corti (North-Holland Publishing, Amsterdam, 1985), p. 303.
[11] G. Onori and A. Santucci, J. Phys. Chem. B **101**, 4662 (1997).
[12] J.M. Corkill, J.F. Goodman, and S.P. Harrold, Trans. Faraday Soc. **60**, 202 (1964).
[13] O. Ortona, V. Vitagliano, L. Paduano, and L. Costantino, J. Colloid Interface Sci. **203**, 477 (1998).
[14] G. Rother, D. Woywod, M. Schoen, and G.H. Findenegg, J. Chem. Phys. **120**, 11864 (2004).
[15] G. Kalies, P. Bräuer, and M. v. Szombathely, J. Colloid Interface Sci. **331**, 329-334 (2009).
[16] D.H. Everett, Trans. Faraday Soc. **61**, 2478 (1965).
[17] S.G. Ash, D. H. Everett, and G. H. Findenegg, Trans. Faraday Soc. **64**, 2645 (1968).
[18] M.M. Telo da Gama and R. Evans, Mol. Phys. **48**, 687 (1983).
[19] Y. Ren, B. Liu, T. Kiryutina, H. Xi, and Y. Qian, Chem. Phys. **448**, 9 (2015).
[20] M. Suttipong, B.P. Grady, and A. Striolo, Phys. Chem. Chem. Phys. **16**, 16388 (2014).
[21] P. Angelikopoulos and H. Bock, J. Phys. Chem. B **112**, 13793 (2008).
[22] D. Müter, M. A. Widmann, and H. Bock, J. Phys. Chem. Lett. **4**, 2153 (2013).
[23] N. Arai, K. Yasuoka, and X.C. Zeng, J. Am. Chem. Soc. **130**, 7916 (2008).
[24] D. Müter, H.O. Sørensen, H. Bock, and S.L.S. Stipp, J. Phys. Chem. C **119**, 10329 (2015).
[25] L. Ambrosone, L. Costantino, G. D'Errico, and V. Vitagliano, J. Colloid Interf. Sci. 190, 286 (1997).
[26] G.H. Findenegg, in *Soft Matter at Aqueous Interfaces*, Lecture Notes in Physics, Vol 917, edited by P.R. Lang and Y. Li (Springer, Heidelberg, 2016), p. 129.
[27] H. Bock and K.E. Gubbins, Phys. Rev. Lett. **92**, 135701 (2004).
[28] G.H. Findenegg and M. Thommes, in *Physical Adsorption: Experiment, Theory and Applications*, edited by J. Fraissard and C.W. Conner, NATO ASI Series C, Vol. 491 (Kluwer, Dordrecht, 1997), p. 151.
[29] E. S. Pagac, D. C. Prieve, and R. D. Tilton, Langmuir 14, 2333 (1998).
[30] S. B. Velegol, B. D. Fleming, S. Biggs, E. J. Wanless, and R. D. Tilton, Langmuir 16, 2548 (2000).
[31] L. Shi, M. Ghezzi, G. Caminati, P. Lo Nostro, B. P. Grady, and A. Striolo, Langmuir 25, 5536 (2009).
[32] S. Wu, L. Shi, L. B. Garfield, R. F. Tabor, A. Striolo, and B. P. Grady, Langmuir 27, 6091 (2011).
[33] M.W.A. Skoda, F. Schreiber, R.M.J. Jacobs, J.R.P. Webster, M. Wolff, R. Dahint, D. Schwendel, and M. Grunze, Langmuir **25**, 4056 (2009).